

Article

Skin Heat Transfer and Thermal Sensation Coupling Model under Steady Stimulation

Yijia Zhou, Hang Yu *, Maohui Luo  and Xiang Zhou

School of Mechanical Engineering, Tongji University, Shanghai 201804, China; 2130278@tongji.edu.cn (Y.Z.); luomaohui@tongji.edu.cn (M.L.); zhouxixiang@tongji.edu.cn (X.Z.)

* Correspondence: yuhang@tongji.edu.cn

Abstract: Thermal sensation prediction models can help to evaluate complex thermal environments and guide the environment conditioning strategy. However, most existing models are established basing on the thermal status of the entire human body or local body parts, failing to reflect thermal sensation generating mechanism or micro-scale (centimeter-scale) thermal sensation. This study put forward a new thermal sensation predicting approach by coupling the skin heat transfer and the thermoreceptor impulse signals. The micro-scale thermal sensitivity data under steady stimuli were applied to bridging the objective heat transfer model and the subjective sensation model. The model contains a one-dimensional skin heat transfer equation and three sensation-generating equations: the thermoreceptor impulse equation, the psychosensory intensity equation, and the thermal sensation equation. The dimension of the skin heat transfer equation was determined through a skin temperature diffusion experiment, and the coefficients of the static/dynamic impulse in the thermoreceptor impulse equation and the thermal sensation equation were obtained through polynomial fitting using thermal sensitivity data. The validated mean absolute percentage error (MAPE) was 0.08 and 0.1 under cooling and heating stimuli, respectively. This new model can predict thermal sensation on the centimeter scale and be applied under different boundary conditions. In the future, the new model can be further developed by testing dynamic stimuli and other boundary conditions so that it can be applied to more complex thermal exposures.

Keywords: thermal sensitivity; thermal sensation; skin heat transfer; thermoreceptor



Citation: Zhou, Y.; Yu, H.; Luo, M.; Zhou, X. Skin Heat Transfer and Thermal Sensation Coupling Model under Steady Stimulation. *Buildings* **2024**, *14*, 547. <https://doi.org/10.3390/buildings14020547>

Academic Editor: Constantinos A. Balaras

Received: 15 January 2024
Revised: 9 February 2024
Accepted: 14 February 2024
Published: 19 February 2024



Copyright: © 2024 by the authors. Licensee MDPI, Basel, Switzerland. This article is an open access article distributed under the terms and conditions of the Creative Commons Attribution (CC BY) license (<https://creativecommons.org/licenses/by/4.0/>).

1. Introduction

Nowadays, people tend to have high demands on thermally comfortable environments. To meet this requirement, researchers have constructed thermal sensation models to predict and evaluate an occupant's thermal comfort status, so that the optimal thermal environment combinations could be determined. In the classic prediction method, thermal sensation or thermal comfort is generally estimated based on the thermal status of the human body or local body parts. Fanger [1] firstly introduced six parameters, namely, air temperature, relative humidity, air velocity, mean radiant temperature, clothing insulation, and metabolic rate, to paraphrase the heat balance equation, that is the classic PMV (predicted mean vote) model. However, the PMV model and its derivatives are not accurate when applied in spatially ununiform and temporally unsteady thermal conditions due to complex physiological and psychological parameters. For the prediction for dynamic thermal sensation and comfort, based on the multi-node thermoregulation model by Stolwijk and Hardy [2], Fiala [3] incorporated the controlled passive system and controlling active system model of the human body to construct the comfort prediction model. Modified models, with a 65-node thermoregulation model and a radiation model by Tanabe [4], and the model constructed by UCB [5] made further improvements. However, these models were constructed mainly by exploring the potential influencing factors of thermal sensation (skin temperature, clothing insulation, etc.) and obtaining thermal sensation directly

through simple regression. They failed to reflect the mechanism of how thermal sensation is generated. Thus, there can be great discrepancies between their predictive results and actual thermal sensation, especially under complex thermal exposures [6–8]. Additionally, these models were constructed on a whole-body or local-body-part scale, while the model at micro-scale, i.e., the centimeter scale, is lacking. The micro-scale thermal sensation data can be beneficial for the development of personal comfort system (PCS) devices which can provide cooling or heating directly to the small spots on the skin, and for guiding the controlling temperature of PCS devices that still remains unanswered [9,10].

When the skin is exposed to external thermal stimuli, the temperature signal transfers from the skin surface to a thermoreceptor beneath the surface, and the thermoreceptor releases an impulse through nerve fibers to the central nervous system, thus generating thermal sensation [11]. This is the mechanism of the generation of thermal sensation, which can be paraphrased as the process of ‘external thermal stimuli–temperature change at thermoreceptor–thermoreceptor impulse–thermal sensation’. Based on this process, thermal sensation can be determined by thermoreceptor temperature and impulse, so the form of the model constructed under this mechanism will not change under different conditions. To date, few models have been constructed based on the full thermal sensation generation process, while there are some research studies on how humans respond to external stimuli based on the partial process. For the process ‘external thermal stimuli–temperature change at thermoreceptor’, researchers have constructed skin heat transfer models. Pennes [12] firstly proposed the BHTE (bioheat transfer equation) to calculate the temperature distribution within the skin layers, considering the skin as an integral consisting of three parts: cells, blood vessels (vascular region), and the extravascular region. To simplify the blood diffusion in BHTE, Vafai [13] overlooked the boundary between the vascular and extravascular region, and proposed the skin structure as a two-part porous medium structure. Based on the porous medium model, Khaled and Vafai [14] investigated the transport application in porous tissue, and Xuan and Roetzel [15] explored the heat transfer between the blood and peripheral tissue using a two-energy equation. Both the BHTE and porous medium model consider the skin as the mono-layer structure, while the real skin is composed of different layers with different thermophysical properties. To simulate heat transfer within the skin precisely, Mahjoob and Vafai [16,17] firstly explored the analytical solution for the tissue and blood temperature profiles and heat transfer correlations to develop the BHTE in a dual-layer skin structure and a multi-layer skin structure. Researchers further explored the multi-layer model in transient heat transfer [18], and extended the model to a two-dimensional [19] or three-dimensional model [20].

For the process ‘temperature change at thermoreceptor–thermoreceptor impulse–thermal sensation’, Hensel [21] discovered that a thermoreceptor converts the temperature signal into an impulse signal. In a steady-state condition, the thermoreceptor only releases a static impulse, while in a transient condition, the thermoreceptor releases a static and a dynamic impulse at the same time. The magnitude of the static impulse depends on the temperature at the thermoreceptor, and that of the dynamic impulse depends on the change in thermoreceptor temperature. Based on the impulse property of the thermoreceptor, Ring and de Dear [22] discovered that the integral of a cold or warm receptor impulse frequency was proportional to PSI (psychosensory intensity), and constructed the thermoreceptor impulse model for the prediction of PSI. Researchers further validated the model under sinusoidal stimuli [23], and compared it with other prediction models [24].

To quantify the skin temperature and thermal sensation at micro-scale, thermal sensitivity, defined as the thermal sensation change caused by a certain thermal stimulus [25], has been used to describe the perception of small regional parts to surrounding thermal environments. Donaldson [26] figured the distribution of cold and heat spots on the back of the left and right hand. Luo [27] mapped the high-density thermal sensitivity of the human body, and explored the variance among different body parts and gender. Our previous studies [28,29] also obtained the thermal sensitivity data of the hand, arm, and face, and

discovered the effect of the initial thermal states, stimulus intensity, and stimulating time on its distribution.

This study further developed Hensel's 'temperature change at thermoreceptor–thermoreceptor impulse–thermal sensation' model by coupling skin heat transfer and the thermoreceptor impulse model. The micro-scale thermal sensitivity data obtained from our previous studies [28,29] were applied to bridging the objective heat transfer model and the subjective sensation model. By doing this, the new model can reflect the full process of the mechanism of how thermal sensation was generated, and predict micro-scale (centimeter-scale) thermal sensation.

The framework of the new model and its comparison with classic thermal sensation prediction models are shown in Figure 1. This paper will firstly construct the model and obtain the unknown coefficients in the model, and then it will discuss its accuracy, potential application, and limitations.

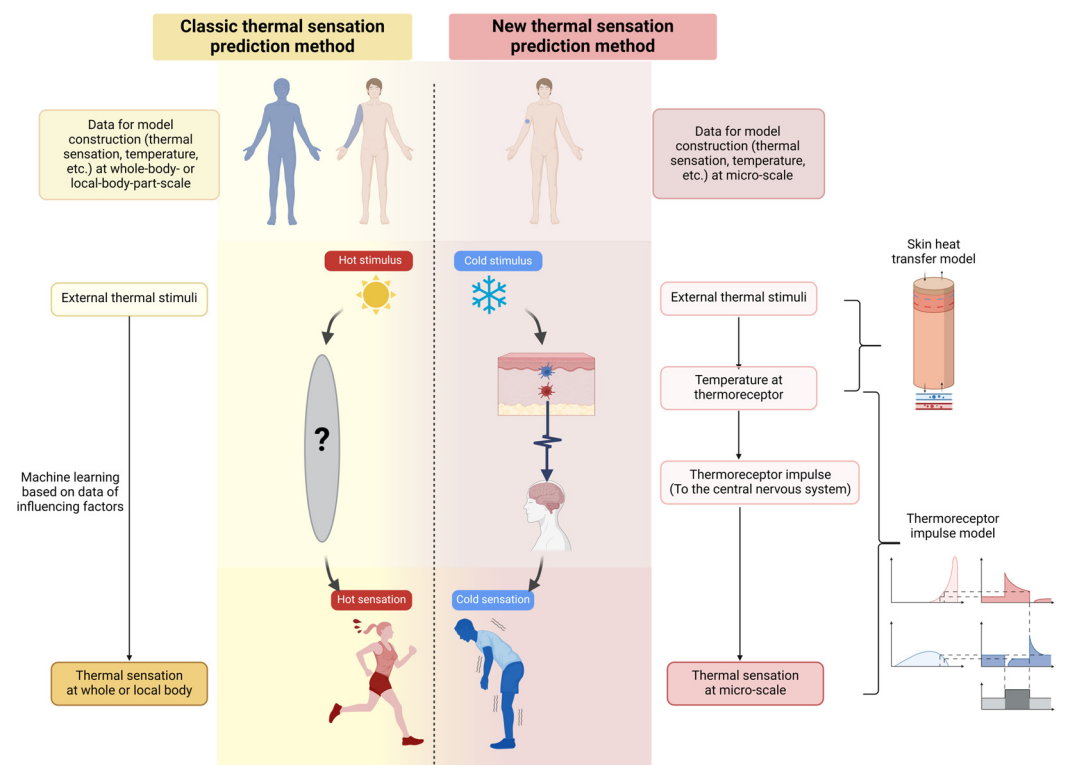


Figure 1. The classic thermal sensation prediction model (left) and the new construction of this study (right) (created with BioRender.com with permission, accessed on 15 February 2024). In the figure of 'Thermoreceptor impulse model', the left part represents static impulse with temperature, the right part represents dynamic impulse with time, and the lowest part represents ambient temperature with time. The red shadow represents impulse at warm receptor, and the blue one represents impulse at cold receptor. In the lowest figure, the darker color represents higher ambient temperature.

2. Methods

The flowchart of the construction of the model is shown in Figure 2. The coupling model includes a skin heat transfer model and a thermoreceptor impulse model. The skin heat transfer model is used to calculate the temperature at the thermoreceptor, and the thermoreceptor impulse model is used to calculate thermal sensation based on thermoreceptor temperature. The dataset for the construction of the model came from the thermal sensation and thermal sensitivity data obtained in the experiments of our previous studies [28,29].

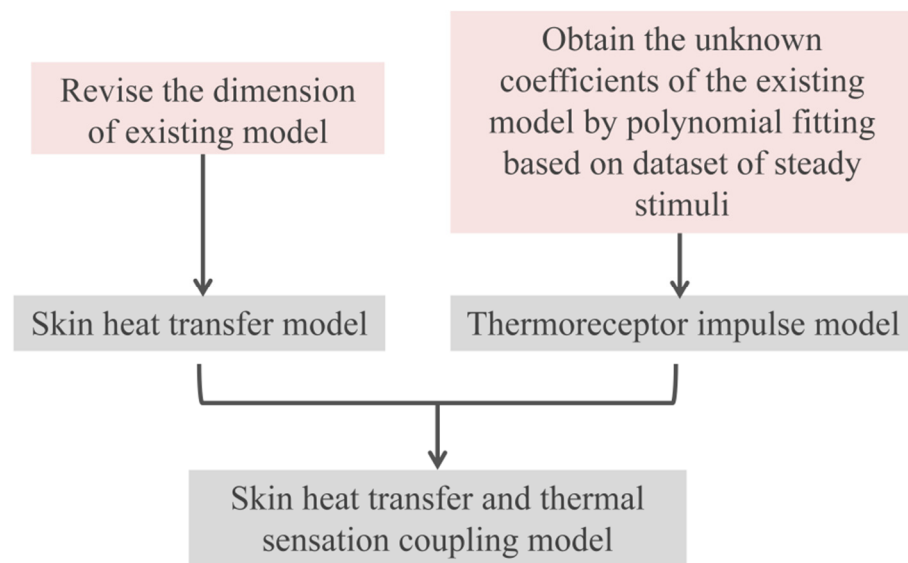


Figure 2. The flowchart of the construction of the model.

2.1. Construction of Skin Heat Transfer Model

Based on the heat balance within the skin, Pennes suggested the BHTE to reflect the heat transfer in each layer of the skin. Since the thermoreceptor is far away from the blood vessel, the equation could overlook the heat from blood flow and metabolism [30]. Thus, the original skin heat transfer equation is described as Equation (1).

$$\lambda \left(\frac{\partial^2 T_{sk}}{\partial x^2} + \frac{\partial^2 T_{sk}}{\partial y^2} + \frac{\partial^2 T_{sk}}{\partial z^2} \right) = c\rho \left(\frac{\partial T_{sk}}{\partial t} \right) \quad (1)$$

where λ is the thermal conductivity (W/m/K). c is the heat capacity (J/kg/K). ρ is density (g/cm^3). t is time (s). T_{sk} is the skin temperature at a certain layer (K). x , y , and z represent the length in a certain direction in three dimensions (m). The original equation considers the heat transfer in three dimensions, while under the short-period stimulation of 10 s [28], the heat transfer in some dimensions may not be so evident. To verify the dimension of the skin heat transfer equation, this paper carried out the skin temperature diffusion experiment to explore the extent of heat transfer after the stimulation in three dimensions.

The apparatus and test spots of the experiment are shown in Figure 3. A shows the stimulation equipment (accuracy of ± 0.1 °C, temperature adjustment between 0 °C and 50 °C, NTE-2A, Physitemp Instruments Inc., Hawthorne, NJ, USA), with its temperature controller (left) and stimulating probe (right). The area of the probe was 1.54 cm^2 with a diameter of 1.4 cm. B shows the infrared camera (accuracy of ± 3 °C, temperature measurement between 0 °C and 400 °C, FLIR ONE Pro, Teledyne FLIR, Wilsonville, OR, USA). C shows the distribution of test spots. The test spots were the dorsum of the hand, the forearm, the upper arm, and the left side of the face. They were the spots with high sensitivity in our previous study [28], and as the center of three body parts, respectively, they could represent the thermal response of each body part. During the experiment, after the subject adapted to the experimental condition, the researcher firstly set the probe temperature to the reference temperature of 32 °C, which could cause local sensation close to 0 [28], conducted neutral stimulation on one test spot for 1 min, and then photographed the temperature distribution around one test spot with the infrared camera. Secondly, the researcher set the probe temperature to -5 °C from the reference temperature to conduct cooling stimulation for 1 min, and then photographed the temperature distribution at the same spot. After the cooling stimulation of all test spots, the researcher conducted heating stimulation following the same process. The infrared photos before and after

the stimulation and the skin temperature data were processed to obtain the diffusivity in three dimensions.

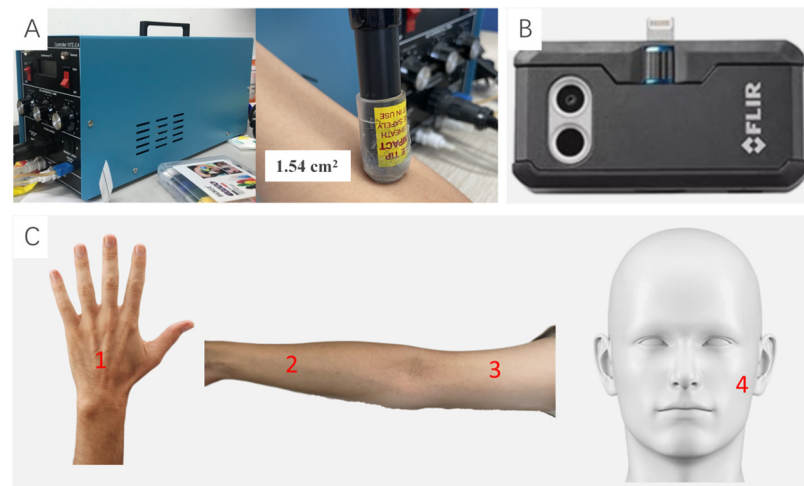


Figure 3. (A) Stimulation equipment. (B) Infrared camera. (C) Test spots. The ‘1-4’ represents the number of each test spot.

The results are shown in Figures 4 and 5. The infrared photos in Figure 4 show the temperature distribution before and after the cooling or heating stimulation of four test spots. It can be concluded that after stimulation, the temperature at the stimulated area would change evidently, while the stimulation hardly diffused to the surrounding area. After cooling stimulation, the skin area with a temperature change would diffuse with an increase in diameter of 0.05 cm, that is, with a diffusivity of 1.039, and after heating stimulation, the area would diffuse with an increase in diameter of 0.04 cm, that is, with a diffusivity of 1.026. Compared with the transverse temperature diffusion on the skin surface, the longitudinal diffusion along with the skin depth could reach the core of the skin, that is, at least 0.54 cm from the skin surface, as shown in Figure 5. Since the transverse diffusivity was only 10% of the longitudinal one, the skin heat transfer model could be considered as a one-dimensional model in the longitudinal direction.

Based on the experimental conclusion, the skin heat transfer equation of this study could be described as Equation (2).

$$\lambda \left(\frac{\partial^2 T_{sk}(x, t)}{\partial x^2} \right) = c\rho \left(\frac{\partial T_{sk}(x, t)}{\partial t} \right) \quad (2)$$

where x represents the depth from the skin surface (m).

To ensure the boundary condition of the skin heat transfer equation, the skin structure model was constructed as shown in Figure 6. The idealized skin structure consists of three parts: epidermis, dermis, and hypodermis [31]. The thermophysical properties of each part are shown in Table 1 [32,33]. Therefore, the depth from the skin surface to the skin core is 5.4 mm. The cold thermoreceptors are mainly distributed at a depth of 0.2 mm and the warm thermoreceptors are at a depth of 0.5 mm [21].

Table 1. Thermophysical properties of epidermis, dermis, and hypodermis.

Skin Layer	Thickness (mm)	Heat Capacity (J/kg/K)	Thermal Conductivity (W/m/K)	Density (g/cm ³)
Epidermis	0.15	3590	0.24	1.2
Dermis	1.5	3300	0.45	1.2
Hypodermis	3.75	2675	0.19	1

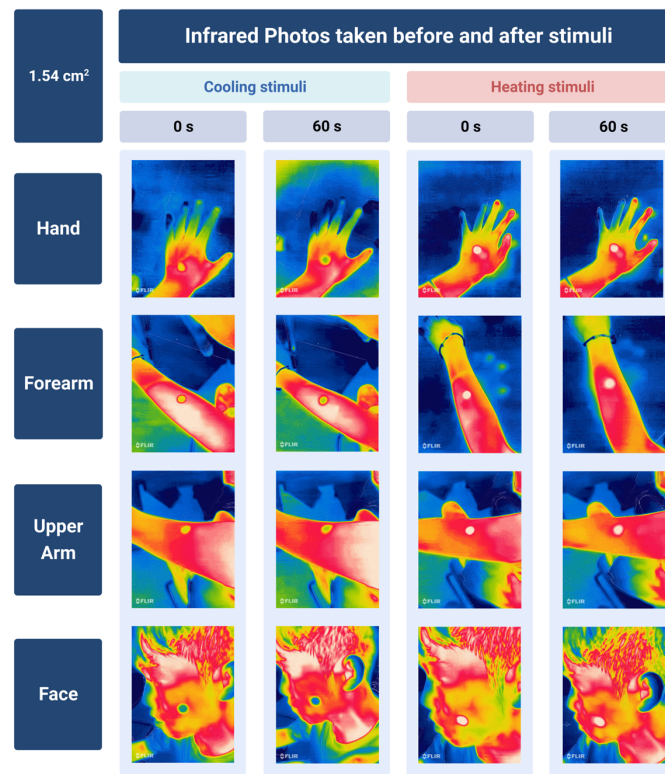


Figure 4. The infrared photos of four test spots before and after the cooling and heating stimuli (created with BioRender.com with permission).

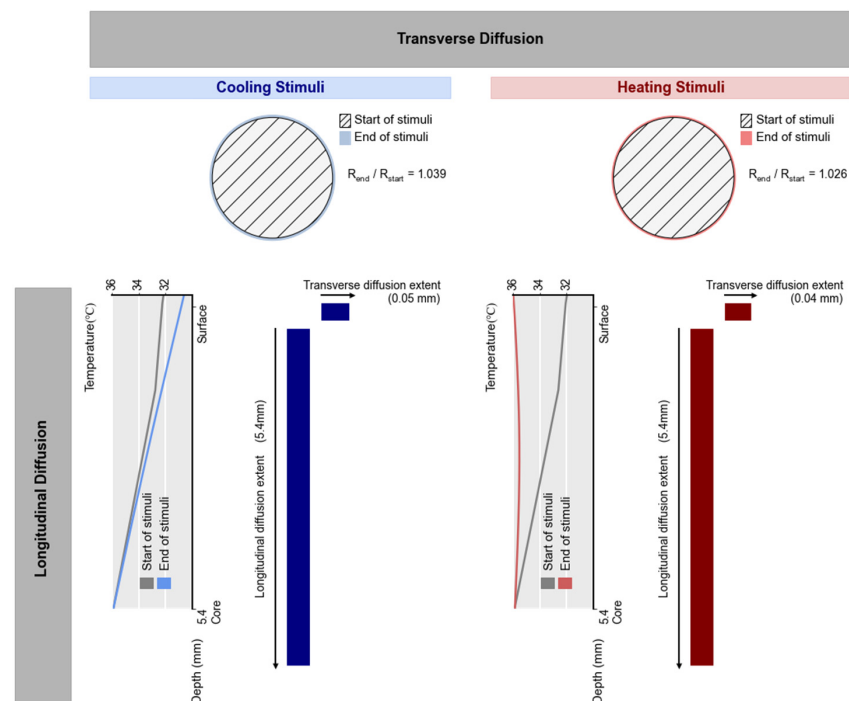


Figure 5. The temperature diffusion before and after the cooling and heating stimuli in the transverse (skin surface) and longitudinal (along skin depth) dimension. In the transverse part, the circle with a slanted shadow represents the skin area with a temperature change at the beginning of stimuli, the one with a blue shadow represents the area after cooling stimuli, and the one with a red shadow represents the area after heating stimuli. In the longitudinal part, the gray line is the temperature distribution before stimuli, and the blue or red line is the distribution after the stimuli.

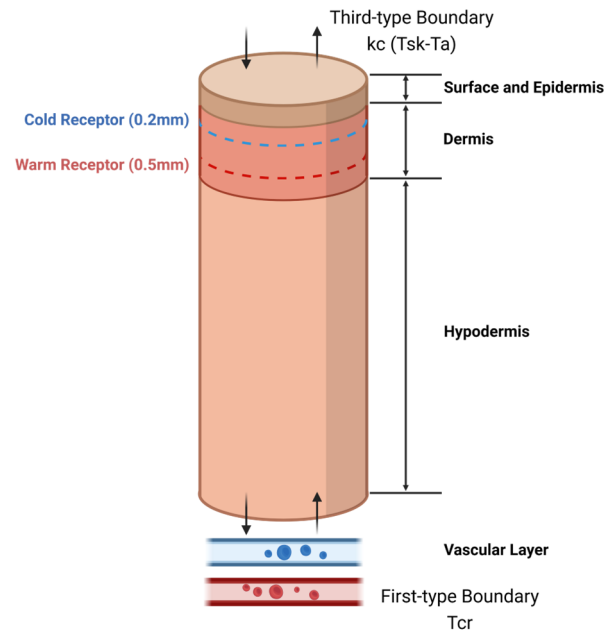


Figure 6. The skin structure model (created with BioRender.com with permission).

This model uses the third-type boundary condition at the skin surface. The boundary condition is described as Equation (3).

$$-\lambda \left(\frac{\partial T_{sk}}{\partial x} \right) = k_c (T_{sk} - T_a) \quad (3)$$

where T_a is the temperature of stimulation (K). k_c is the heat transfer coefficient between the stimulation probe and the skin surface ($W/m^2/K$), and it can be calculated using Equation (4) [33].

$$k_c = 1.25 \lambda_c \frac{\Delta a_c}{\varepsilon_c} \left(\frac{P_c}{H_c} \right)^{0.95} \quad (4)$$

where λ_c is the harmonic mean thermal conductivity ($W/m/K$). Δa_c is the average surface asperity slope of the contact interface (rad). ε_c is the average surface roughness of the contact interface (μm). The three parameters were calculated using Equations (5)–(7). The subscript 1 and 2 represent the parameters of the stimulation probe and skin surface, respectively. P_c is the contact pressure (kPa). H_c is the microhardness of the contact material (MPa). The data of the parameters of the stimulation probe and skin surface are listed in Table 2 [33].

$$\lambda_c = \frac{2\lambda_1\lambda_2}{\lambda_1 + \lambda_2} \quad (5)$$

$$\Delta a_c = \sqrt{\Delta a_1^2 + \Delta a_2^2} \quad (6)$$

$$\varepsilon_c = \sqrt{\varepsilon_1^2 + \varepsilon_2^2} \quad (7)$$

Table 2. Thermophysical properties of the skin surface and stimulation probe.

Material	Thermal Conductivity (W/m/K)	Surface Roughness (μm)	Surface Asperity Slope (rad)	Contact Pressure (kPa)	Microhardness (Mpa)
Skin surface	0.24	21.69	0.3	0.8	0.1225
Stimulation probe (stainless steel 304)	14.986	0.008	0.009	--	--

At the skin core, the model uses the first-type boundary condition. The core temperatures of the hand, arm, and face are shown in Table 3 [34].

Table 3. Core temperatures of the hand, arm, and face.

Body Part	Core Temperature (°C)
Hand	35.05
Arm	35.87
Face	37.46

2.2. Construction of Thermoreceptor Impulse Model

Based on the thermoreceptor impulse theory by Hensel [21], Ring and de Dear [22] explored the mathematical relationship between the thermoreceptor impulse and thermal sensation. Under the external thermal stimulation, the thermoreceptor releases both a static and a dynamic impulse. Thus, the total impulse is described as Equation (8).

$$R(t) = K_s(T_{\text{rec}}(t) - T_{\text{rec}}(0)) + K_d \frac{\partial T_{\text{rec}}(t)}{\partial t} \quad (8)$$

where R is the total thermoreceptor impulse (HZ). T_{rec} is the temperature at the thermoreceptor (K). K_s is the static coefficient, and K_d is the dynamic coefficient. According to existing research [23], K_s is related to the initial thermoreceptor temperature before stimulation, and K_d is related to stimulus intensity and the change rate of stimulus intensity. Since the dataset for the steady model was obtained in the experiment with only one type of stimulus intensity (-5 °C under cooling stimulation and 5 °C under heating stimulation) and only one type of initial stimulation temperature (32 °C), K_s and K_d of the steady model were both constants. To reflect the difference of thermal sensory intensity at different body parts, the equation should multiply the thermal sensitivity as the areal summation factor [35]. The micro-scale thermal sensitivity in the dataset can also reflect the thermal response of micro-scale test spots. Thus, the total impulse equation of the steady model can be described as Equation (9).

$$R(t) = TS(C_1(T_{\text{rec}}(t) - T_{\text{rec}}(0)) + C_2 \frac{\partial T_{\text{rec}}(t)}{\partial t}) \quad (9)$$

where TS is the thermal sensitivity of each test spot (1/K). C_1 and C_2 are constants representing K_s and K_d , respectively.

The PSI is calculated by integrating the total impulse for the first 20 s of stimulation, and thermal sensation is proportional to PSI [36]. The correlation can be described as Equations (10) and (11), where TSV is the thermal sensation vote, and C_3 is the constant coefficient. Thus, the thermoreceptor impulse model is the combination of Equations (9)–(11). To obtain the coefficients C_1 , C_2 , and C_3 , the training set of the thermal sensation and thermal sensitivity data will be used to train the model.

$$\text{PSI} = \int_0^{20} R(t)dt \quad (10)$$

$$\text{TSV} = C_3\text{PSI} \quad (11)$$

2.3. Dataset for the Model Construction

The data of thermal sensation and thermal sensitivity for the construction of the model under steady stimulation were obtained from the experiment on the hand, arm, and face [29]. A total of 50 subjects (25 male, 25 female) were invited to participate in the experiments under thermally neutral conditions. They were healthy college students, about 20 years old, living in Shanghai for more than 3 months before the experiment. To ensure that the body surface area of the male and female subjects could match to avoid its

influence on the thermal sensation votes [37], the weights and heights of the subjects were filtered using Equation (12), where A is the body surface area (m^2), H is the height (m), and m is the weight (kg).

$$A = 0.202m^{0.425}H^{0.725} \quad (12)$$

During the experiment, 57 test spots of the hand, 25 test spots of the arm, and 25 test spots of the face were stimulated, firstly under a reference temperature of $32\text{ }^\circ\text{C}$, that is, the temperature producing a thermal sensation vote of 0, and then under a cooling stimulation of $27\text{ }^\circ\text{C}$ ($-5\text{ }^\circ\text{C}$ from the reference) or a heating stimulation of $37\text{ }^\circ\text{C}$ ($+5\text{ }^\circ\text{C}$ from the reference). In the meantime, the subjects recorded thermal sensation before and after the stimulation at the test spot, and the researcher recorded the change in skin temperature of the test spot. Thermal sensitivity was calculated as the change in thermal sensation vote divided by the change in skin temperature. The bar charts of the thermal sensation and thermal sensitivity of the hand, arm, and face are shown in Figure 7. A total of 80% of the data were used for the training set, and 20% were used for the test set.

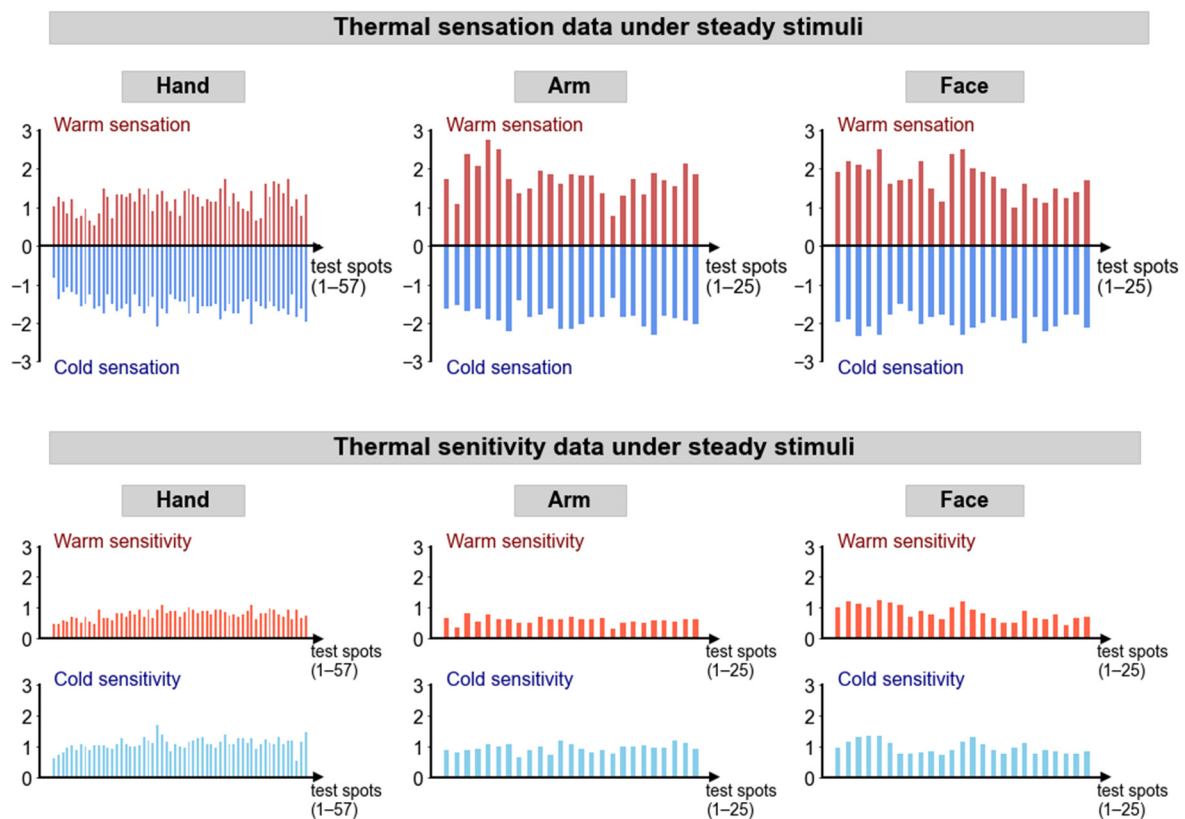


Figure 7. The data of the thermal sensation and thermal sensitivity of the hand, arm, and face. In the upper figures, the red represents warm sensation, and the blue represents cold sensation. In the lower figures, the red represents warm sensitivity, and the blue represents cold sensitivity.

2.4. Data Processing

The thermal sensation predicting process of this model is shown in the flowchart in Figure 8. This paper analyzed the skin temperature distribution under stimulation through the calculation of the skin heat transfer model, obtained the unknown coefficients of the thermoreceptor impulse equations to construct the complete skin heat transfer coupling model based on the training set, and validated the model based on the test set. MATLAB (R2020b, The MathWorks, Inc., Natick, MA, USA) and Python were used for the construction and validation of the model. In our programming, the initial skin temperature of each test spot was input to simulate the temperature distribution within the skin, and

then the stimulating temperature was input to simulate how temperature changes in 20 s at each depth of the skin using the finite difference method.

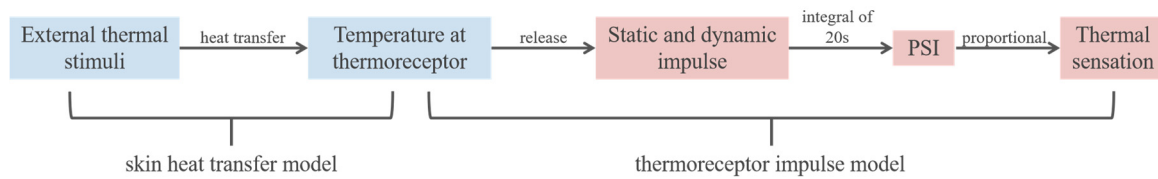


Figure 8. The predicting process of the model.

3. Results

3.1. Skin Temperature Distribution after Stimulation

The average skin temperature distribution after the steady cooling and heating stimulation is shown in Figure 9. The depth of 0 mm is the skin surface, and the depth of 5.4 mm is the skin core. The core temperature was the average of the hand, arm, and face at 36.1 °C. Since the skin heat transfer model was a one-dimensional model, the temperature remained the same at the same skin layer, and changed only with the depth. After cooling stimulation, the average skin surface temperature was 31.5 °C, and increased with the depth almost linearly to the core temperature. After heating stimulation, the average skin temperature at the surface was 35 °C, and firstly decreased to the lowest point at the depth of 1.9 mm, then increased to the core temperature. This may be because in a stimulation lasting only 20 s, the temperature within the skin was not sufficiently heated to the stable state as the linear distribution, and the heating rate of the skin layers near the heat source (stimulating probe at the skin surface and blood flow at the skin core) was higher than the ones far from the heat source.

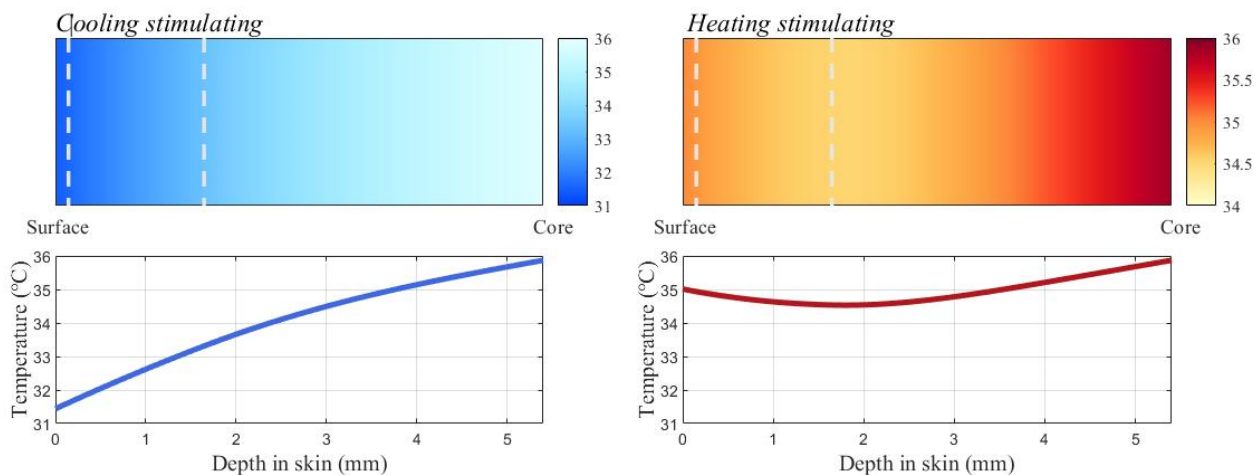


Figure 9. The skin temperature distribution with the depth of the skin.

3.2. Thermoreceptor Temperature Change with Time

The change in thermoreceptor temperature with time under cooling and heating stimulation is shown in Figure 10. The left part of the figure shows the temperature of the cold receptor, and the right part shows that of the warmth receptor. Before the stimulation, since the cold receptor was located at a shallower depth than the warmth receptor, the initial cold receptor temperature was 32 °C, slightly lower than the warmth receptor which was 32.2 °C. During stimulation, the cold receptor temperature decreased gradually, then remained stable after 15 s from the beginning of stimulation, while the warmth receptor temperature continued to increase throughout the stimulation. This may also be because of the insufficient heating during the short-time stimulation, lasting only 20 s.

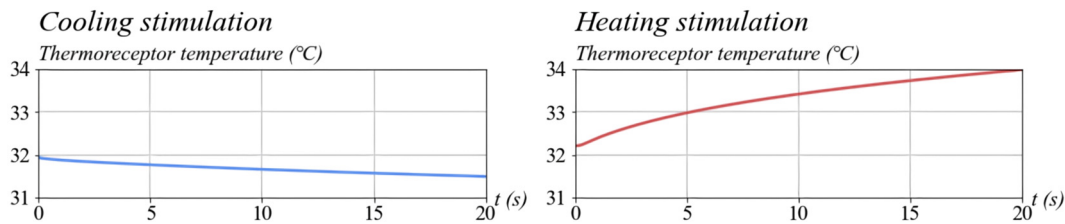


Figure 10. Temperature change with time of the cold and warmth receptor.

3.3. Fitting of the Model

To obtain the unknown coefficients C_1 , C_2 , and C_3 to complete the steady thermoreceptor impulse model, the training set of thermal sensation and thermal sensitivity data and the simulated thermoreceptor temperature data from the skin heat transfer model were used for nonlinear polynomial fitting. The fitting results are shown in Figure 11. The fitting curves were represented by the cold and warm sensation calculated by the fitted skin heat transfer coupling model based on the training set. For cooling stimulation, the coefficients C_1 , C_2 , and C_3 were -3 , -12.6 , and 0.0499 , respectively, and for heating stimulation, they were 2.4 , 6.7 , and 0.0466 , respectively. The determination coefficient (R_2) of the model under cooling stimulation was 0.85 , and under heating stimulation it was 0.88 , indicating a good fitting result.

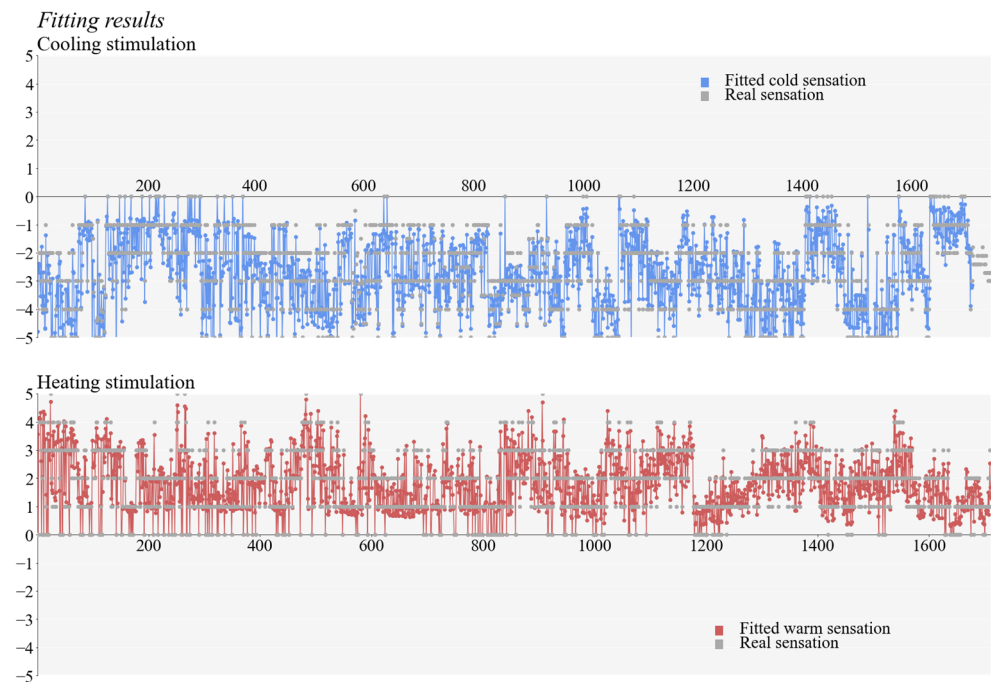


Figure 11. Model fitting results.

3.4. Validation of the Model

To explore the accuracy of the skin heat transfer model, the test set of the data was used to validate the steady and dynamic model. The validation results are shown in Figure 12. Each type of stimulation took 20% of the experimental data as the test set. The test thermal sensitivity data were applied to calculate the predictive thermal sensation, and the test thermal sensation data were applied for the comparison between the predictive and real thermal sensation. As shown in the figure, the MAPE (mean absolute percentage error) was 0.03 under cooling stimulation, and 0.05 under heating stimulation. Thus, the model could be considered to be accurate in predicting thermal sensation under steady and dynamic stimulation.

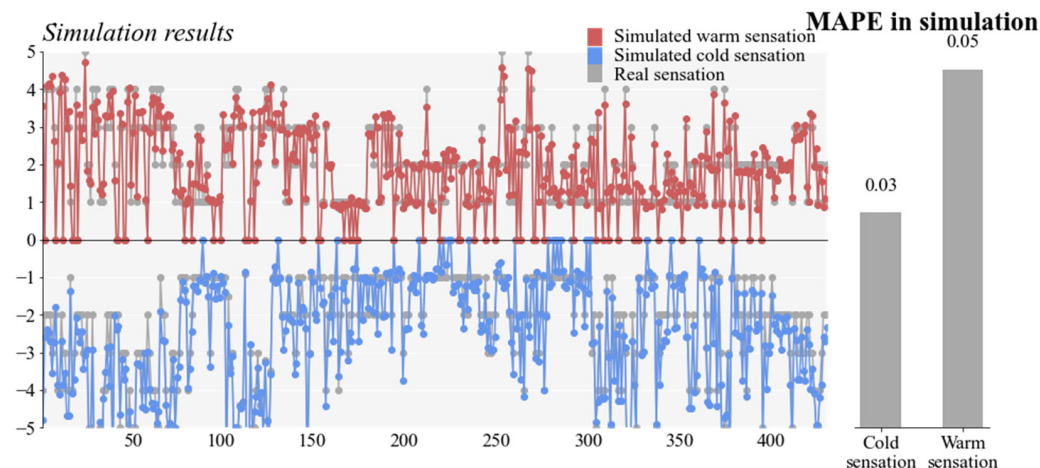


Figure 12. Model validation results.

4. Discussion

4.1. Potential Application

The skin heat transfer coupling model constructed in this study can be applied to the micro-scale thermal sensation prediction under different complex exposures. The existing thermal sensation prediction models are mostly constructed using regression under only one type of exposure, e.g., a room with air conditioning. Therefore, when there are various exposures, e.g., an air-conditioned room with a fan, the influencing factors for thermal sensation change and the regression functions are unavailable. However, the model in this study can be applied in different thermal conditions, since its input only contains initial skin temperature and external stimulating temperature. Additionally, it can be applied to the development of small-scale personal comfort system (PCS) devices. Such devices can be worn by the user to regulate skin temperature in the small areas where they are worn, like wrist-bands and neck-worn fans for smaller scales [38,39], to improve thermal comfort. By using this model, the user can better regulate the stimulating temperature of the device to enhance micro-scale satisfaction.

4.2. Limitations

This paper constructed a skin heat transfer model and a thermoreceptor impulse model, and validated their performance in thermal sensation prediction under steady stimuli. However, whether the skin temperature simulated by the skin heat transfer model and the impulse simulated by the thermoreceptor impulse model were accurate is unknown. To validate either of the two models, the data of the real temperature within the skin and the real impulse released by the thermoreceptor were required, but the current apparatus for these measurements was unavailable. Additionally, this study only considered steady and contact stimuli without considering dynamic changing-temperature stimuli or non-contact stimuli such as the radiative and convective stimuli. Since the model was constructed using the third-type boundary condition at the skin surface, it has the potential to be developed in a transient and non-contact environment, such as draught, radiation, or showering comfort studies.

5. Conclusions

This study constructed the skin heat transfer and thermal sensation coupling model under steady stimulation by reconstructing the skin heat transfer model and the thermoreceptor impulse model, and validated the model using the test set of experimental data. The model used the fixed temperature boundary condition at the skin surface, and thus the input for the model only requires external stimulation. This study obtained conclusions as follows.

First, in the stimulation time of 1 min, skin temperature diffused with an increase in diameter of 0.05 cm under cooling stimulation and 0.04 under heating stimulation at the skin surface, far less than the diffusing depth of 0.54 cm in the longitudinal direction.

Second, the temperature distribution of the skin was stable at the end of stimulation under cooling stimulation, while it still changed under heating stimulation. The temperature of the cold receptor remained stable after 15 s from the beginning of stimulation, while the warmth receptor temperature continued to increase.

Third, the R^2 of the model indicates a good fitting result, and the MAPE of the model indicates high accuracy in the prediction.

Author Contributions: Methodology, Y.Z. and M.L.; Software, Y.Z.; Resources, Y.Z. and M.L.; Data curation, Y.Z.; Writing—original draft, Y.Z.; Writing—review and editing, M.L., H.Y. and X.Z.; Funding acquisition, M.L. and H.Y. All authors have read and agreed to the published version of the manuscript.

Funding: The research was supported by the National Natural Science Foundation of China (No. 52078355, No. 52108086, No. 51578386), the China National Key R&D Program during the 14th Five-year Plan Period (No. 2022YFC3801500), the National Engineering Research Center of New Energy Vehicles and Power Systems, and the Shanghai Key Lab of Vehicle Aerodynamics and Vehicle Thermal Management Systems.

Data Availability Statement: The data presented in this study are available upon request from the corresponding author. The original data are not publicly available.

Conflicts of Interest: The authors declare no conflicts of interest.

References

1. Fanger, P.O. *Thermal Comfort, Analysis and Applications in Environmental Engineering*; Danish Technical Press: Copenhagen, Denmark, 1970.
2. Stolwijk, J.A.J.; Hardy, J.D. Temperature regulation in man—A theoretical study. *Pflüger's Arch. Gesamte Physiol. Menschen Tiere* **1966**, *291*, 129–162. [[CrossRef](#)]
3. Fiala, D. *Dynamic Simulation of Human Heat Transfer and Thermal Comfort*; De Montfort University: Leicester, UK, 1998.
4. Tanabe, S.-i.; Kobayashi, K.; Nakano, J.; Ozeki, Y.; Konishi, M. Evaluation of thermal comfort using combined multi-node thermoregulation (65MN) and radiation models and computational fluid dynamics (CFD). *Energy Build.* **2002**, *34*, 637–646. [[CrossRef](#)]
5. Huizenga, C.; Hui, Z.; Arens, E. A model of human physiology and comfort for assessing complex thermal environments. *Build. Environ.* **2001**, *36*, 691–699. [[CrossRef](#)]
6. Du, H.; Lian, Z.; Lai, D.; Duanmu, L.; Zhai, Y.; Cao, B.; Zhang, Y.; Zhou, X.; Wang, Z.; Zhang, X.; et al. Evaluation of the accuracy of PMV and its several revised models using the Chinese thermal comfort Database. *Energy Build.* **2022**, *271*, 112334. [[CrossRef](#)]
7. Xie, Y.; Huang, T.; Li, J.; Liu, J.; Niu, J.; Mak, C.M.; Lin, Z. Evaluation of a multi-nodal thermal regulation model for assessment of outdoor thermal comfort: Sensitivity to wind speed and solar radiation. *Build. Environ.* **2018**, *132*, 45–56. [[CrossRef](#)]
8. Zhou, X.; Liu, S.; Liu, X.; Lin, X.; Qing, K.; Zhang, W.; Li, J.; Dong, J.; Lai, D.; Chen, Q. Evaluation of Four Models for Predicting Thermal Sensation in Chinese Residential Kitchen. In *E3S Web Conference*; EDP Sciences: Les Ulis, France, 2019; Volume 111.
9. Luo, M.; Arens, E.; Zhang, H.; Ghahramani, A.; Wang, Z. Thermal comfort evaluated for combinations of energy-efficient personal heating and cooling devices. *Build Environ.* **2018**, *143*, 206–216. [[CrossRef](#)]
10. Wang, Z.; Warren, K.; Luo, M.; He, X.; Zhang, H.; Arens, E.; Chen, W.; He, Y.; Hu, Y.; Jin, L.; et al. Evaluating the comfort of thermally dynamic wearable devices. *Build Environ.* **2020**, *167*, 106443. [[CrossRef](#)]
11. Djongyang, N.; Tchinda, R.; Njomo, D. Thermal comfort: A review paper. *Renew. Sustain. Energy Rev.* **2010**, *14*, 2626–2640. [[CrossRef](#)]
12. Pennes, H.H. Analysis of Tissue and Arterial Blood Temperatures in the Resting Human Forearm. *J. Appl. Physiol.* **1948**, *1*, 93–122. [[CrossRef](#)] [[PubMed](#)]
13. Vafai, K. *Porous Media: Applications in Biological Systems and Biotechnology*; Taylor & Francis Group: Milton, UK, 2010.
14. Khaled, A.R.A.; Vafai, K. The role of porous media in modeling flow and heat transfer in biological tissues. *Int. J. Heat Mass Transf.* **2003**, *46*, 4989–5003. [[CrossRef](#)]
15. Xuan, Y.; Roetzel, W. Bioheat equation of the human thermal system. *Chem. Eng. Technol.* **1997**, *20*, 268–276. [[CrossRef](#)]
16. Mahjoob, S.; Vafai, K. Analytical characterization of heat transport through biological media incorporating hyperthermia treatment. *Int. J. Heat Mass Transf.* **2009**, *52*, 1608–1618. [[CrossRef](#)]
17. Mahjoob, S.; Vafai, K. Analysis of Bioheat Transport Through a Dual Layer Biological Media. *J. Heat Transf.* **2009**, *132*, 031101. [[CrossRef](#)]

18. Becker, S.M. One-Dimensional Transient Heat Conduction in Composite Living Perfuse Tissue. *J. Heat Transf.* **2013**, *135*, 071002. [[CrossRef](#)]
19. Sarkar, D.; Haji-Sheikh, A.; Jain, A. Temperature distribution in multi-layer skin tissue in presence of a tumor. *Int. J. Heat Mass Transf.* **2015**, *91*, 602–610. [[CrossRef](#)]
20. Ma, J.; Yang, X.; Sun, Y.; Yang, J. Thermal damage in three-dimensional vivo bio-tissues induced by moving heat sources in laser therapy. *Sci. Rep.* **2019**, *9*, 10987. [[CrossRef](#)]
21. Hensel, H. Thermoreception and temperature regulation. *Monogr. Physiol. Soc.* **1981**, *38*, 1–321.
22. Ring, J.W.; de Dear, R. Temperature Transients: A Model for Heat Diffusion through the Skin, Thermoreceptor Response and Thermal Sensation. *Indoor Air* **1991**, *1*, 448–456. [[CrossRef](#)]
23. Ring, J.W.; de Dear, R.; Melikov, A. Human thermal sensation: Frequency response to sinusoidal stimuli at the surface of the skin. *Energy Build.* **1993**, *20*, 159–165. [[CrossRef](#)]
24. Parkinson, T.; Zhang, H.; Arens, E.; He, Y.; de Dear, R.; Elson, J.; Parkinson, A.; Maranville, C.; Wang, A. Predicting thermal pleasure experienced in dynamic environments from simulated cutaneous thermoreceptor activity. *Indoor Air* **2021**, *31*, 2266–2280. [[CrossRef](#)]
25. McIntyre, D.A. *Indoor Climate*; Applied Science Publishers Ltd.: London, UK, 1980; Volume 443.
26. Donaldson, H.H. On the temperature-sense. *Mind* **1885**, *10*, 398–416. [[CrossRef](#)]
27. Luo, M.; Wang, Z.; Zhang, H.; Arens, E.; Filingeri, D.; Jin, L.; Ghahramani, A.; Chen, W.; He, Y.; Si, B. High-density thermal sensitivity maps of the human body. *Build Environ.* **2020**, *167*, 106435. [[CrossRef](#)]
28. Zhou, Y.; Yu, H.; Xu, S.; Luo, M.; Zhou, X. High-density thermal sensitivity of the hand under different thermal states and stimulus intensities. *Indoor Air* **2022**, *32*, e13089. [[CrossRef](#)]
29. Zhou, Y.; Luo, M.; Yu, H.; Zhou, X. Evaluating the dynamic thermal sensitivities of human body with high-dense contacting thermal stimuli. *Indoor Built Environ.* **2023**, 1420326X231201847. [[CrossRef](#)]
30. Dufour, A.; Després, O.; Pebayle, T.; Lithfous, S. Thermal sensitivity in humans at the depth of thermal receptor endings beneath the skin: Validation of a heat transfer model of the skin using high-temporal resolution stimuli. *Eur. J. Appl. Physiol.* **2020**, *120*, 1509–1518. [[CrossRef](#)] [[PubMed](#)]
31. Wang, S.; Yu, R.-X.; Fan, W.; Li, C.-X.; Fei, W.-M.; Li, S.; Zhou, J.; Hu, R.; Liu, M.; Xu, F.; et al. Detection of skin thickness and density in healthy Chinese people by using high-frequency ultrasound. *Ski. Res. Technol.* **2023**, *29*, e13219. [[CrossRef](#)] [[PubMed](#)]
32. Gowrishankar, T.R.; Stewart, D.A.; Martin, G.T.; Weaver, J.C. Transport lattice models of heat transport in skin with spatially heterogeneous, temperature-dependent perfusion. *BioMedical Eng. OnLine* **2004**, *3*, 42. [[CrossRef](#)] [[PubMed](#)]
33. Zhang, A.; Pang, D.; Wang, B.; Wang, J. Dynamic responses of wearable thermoelectric generators used for skin waste heat harvesting. *Energy* **2023**, *262*, 125621. [[CrossRef](#)]
34. Takahashi, Y.; Nomoto, A.; Yoda, S.; Hisayama, R.; Ogata, M.; Ozeki, Y.; Tanabe, S.-i. Thermoregulation model JOS-3 with new open source code. *Energy Build.* **2021**, *231*, 110575. [[CrossRef](#)]
35. de Dear, R.J.; Ring, J.W.; Fanger, P.O. Thermal Sensations Resulting From Sudden Ambient Temperature Changes. *Indoor Air* **1993**, *3*, 181–192. [[CrossRef](#)]
36. Molinari, H.H.; Greenspan, J.D.; Krenshalo, D.R. The effects of rate of temperature change and adapting temperature on thermal sensitivity. *Sens. Process.* **1977**, *1*, 354–362.
37. *ASHRAE 55:2020*; Thermal Environmental Conditions for Human Occupancy. American Society of Heating Refrigerating and Air-Conditioning Engineers (ASHRAE): Atlanta, GA, USA, 2020.
38. Reon Pocket. Available online: <https://popbee.com/tag/reon-pocket/> (accessed on 10 January 2024).
39. Embr Wave. Available online: <https://embrlabs.com/embr-wave/> (accessed on 10 January 2024).

Disclaimer/Publisher’s Note: The statements, opinions and data contained in all publications are solely those of the individual author(s) and contributor(s) and not of MDPI and/or the editor(s). MDPI and/or the editor(s) disclaim responsibility for any injury to people or property resulting from any ideas, methods, instructions or products referred to in the content.